Electromagnetic Coupling Analysis of Transient Excitations of Rectangular Cavity through Slot using TD-EFIE with Laguerre Polynomials as Temporal Basis Functions

D. Omri and T. Aguili

Syscom Laboratory
National Engineering School of Tunis, BP 37, Belvédère, 1002, Tunis, Tunisia
omridorsaf@yahoo.fr

Abstract ─ This paper presents an electromagnetic coupling analysis of transient waves excited a rectangular cavity containing an interior scatterer coupled to an external scatterer through a slot. Based on the equivalence principle, time domain integral equations are established by enforcing the boundary conditions on the internal and external scatterers, the slot and the cavity walls. The method of moments is applied in space and time domains to solve the developed system of integral equations. The unknown coefficients of the electric and magnetic currents are approximated by the triangular piecewise functions associated with Dirac function as space basis. To obtain accurate and stable solutions, the Laguerre functions are used as temporal basis. Numerical results involving the coupling effects between the cavity components are investigated. The numerical results are found to be in good agreement with EM theory and literature.

Index Terms ─ Coupling effect, equivalence principle, Laguerre functions, MoM, piecewise triangular functions, slot, TD-EFIE, transient electric and magnetic currents.

I. INTRODUCTION

In electromagnetic compatibility, it is interesting to model the coupling through a slot-aperture backed by a rectangular cavity. When the cavity is excited by internal field source, it acts as an aperture antenna that radiates in external region. The problem of coupling between this radiation element and some components close to the cavity can influence the integrity of communication system. Another typical problem is the evaluation of the current induced by incident electromagnetic fields through an aperture because this current may damage some critical components in the system. Also the response of the cavity through the slot can damage the equipments at the side of cavity.

In order to tackle the two problems, many researchers have developed a lot of frequency domain methods for many cavity designs [1]-[5]. But, for the defense and security reasons, the transient response of these problems can be depicted easily in time domain.

The transient response of the cavity through an aperture is obtained primarily by Inverse Fourier Transforms (IFT) [6]. An exact solution using this method cannot be found. Reference [7] solves the transient problem by using the singularity expansion method (SEM). Recently, the integral equations are formulated and solved in time domain using a time stepping technique [8]-[11]. That later suffers from the late-time instabilities.

In this paper, we consider a communication system composed on a rectangular cavity backed slot containing an internal (probe) and external (thin wire antenna) scatterers. The latters are coupled through the slot.

The aim of this work is to develop a general system of Time Domain Electric Field Integral Equations (TD-EFIE) based on the equivalence principle and the appropriate boundary conditions. In fact, when the cavity is excited through the slot by internal and/or external transient electromagnetic waves, we can apply the developed integral equations system to predict the transient responses of the structure and to study the physical coupling effects between the component of the designed system.

In order to solve the proposed TD-EFIE by applying the Method of Moments (MoM) [12], we introduce a spatial and temporal testing procedures. The piecewise triangular functions [13] associated with Dirac functions are used as spatial basis functions. The present paper sets out to present an accurate technique to obtain stable solutions of the obtained TD-EFIE system using Laguerre polynomials as temporal basis functions [14]-[18]. The transient responses of the structure are compared to the results obtained by applying the B-Spline functions as a temporal basis [22]. In fact, an accurate comparison of the two time approaches (Laguerre scheme and B-Spline scheme) in terms of complexity, accuracy and stability was presented in [22].

Submitted On: January 31, 2015
Accepted On:January 9, 2016

In this work and based on the results stemming from this comparison, a coupling between the thin wire antenna and the probe through the slot is studied using Laguerre functions. The space distributions of the currents are presented.

The paper is divided in four sections. Section II presents the integral equations formulation in the time domain and the method of solving these equations. Numerical results are given in Section III. Section IV concludes the paper.

II. TD-EFIE FORMULATION

The geometry of the analyzed problem is depicted in Fig. 1, which consists of a cavity with a slot on its wall, located in the X-Y plan. A linear electric probe of the length l_p at the position (x_P, y_P) is located inside the cavity at the distance D of the slot. Outside the cavity, we consider a thin wire antenna of the length l_A vertically placed at the distance d from the cavity and located in parallel to the slot at the position (x_A, y_A).

To investigate the radiation characteristics of the structure, we assume that:

- The cavity walls, the antenna and the probe are considered as perfect conductors and very thin.
- The antenna is excited by $\vec{E}_{01} = E_{01}\vec{y}$.
- The probe is excited by $\vec{E}_{02} = E_{02}\vec{y}$.

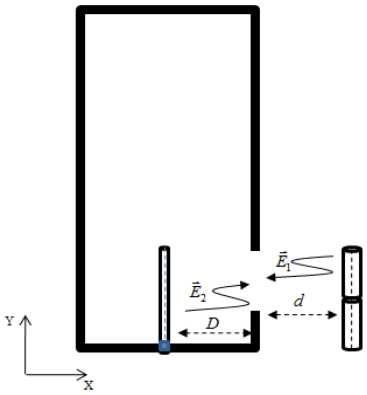

Fig. 1. The geometry of the problem.

By involving the equivalence principle [19], an equivalent surface replaces the physical structure with equivalent magnetic current density radiating in free space over the slot. References [20]-[21] have demonstrated that the magnetic current density is moving an infinitesimal distance away from equivalent surface. Mathematical analysis of this step shows that the slot can be short-circuited. Therefore, two coupled-equivalent problems are established (Fig. 2). In both the external and internal equivalent problems, we retain the sources in the region of interest. In Fig. 3, we represent the different domains:

- $D = \Omega_1 \cup \Omega_3 \cup \Omega_4$ the external analyzed domain.
- $D = \Omega_2 \cup \Omega_3 \cup \Omega_4$ the internal analyzed domain.

Where Ω_1 is the surface of the antenna; Ω_2 is the surface of the probe; Ω_3 is the equivalent domain replacing the slot; Ω_4 is equivalent surface replacing the cavity walls. In fact, the domain Ω_3 is the sub-domain infinitesimally close to, but not coincident with Ω_4. Over it remains not null the equivalent magnetic current.

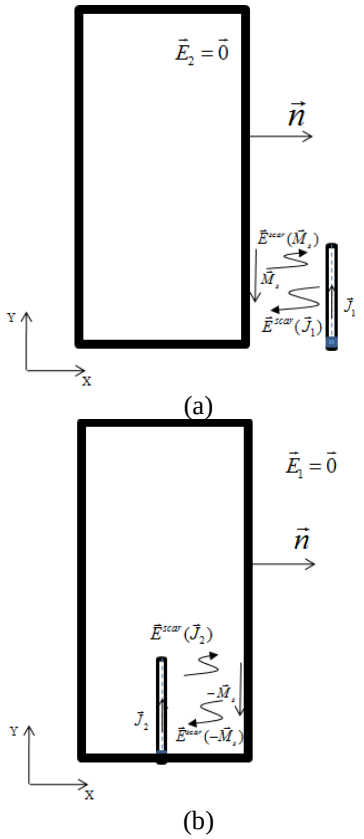

Fig. 2. The equivalent problem: (a) equivalent external problem, and (b) equivalent internal problem.

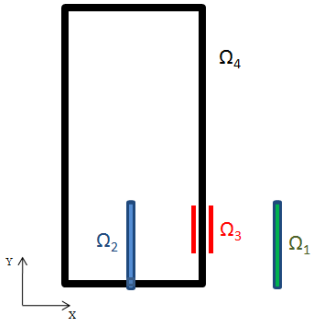

Fig. 3. The different domains: cavity walls, slot, antenna and probe.

The external problem contains the equivalent magnetic current density $\vec{M}_s$ and the unknown electric current $\vec{J}_1$ (Fig. 2 (a)). The fields inside Ω_4 are zero and outside are equal to the radiation produced by the incident field $\vec{E}_{01}$ and scattered fields induced by $\vec{M}_s$ and $\vec{J}_1$. These fields must satisfy the following boundary condition:

$$\vec{M}_s = -\vec{n} \times \vec{E}_1, \tag{1}$$

where

$$\vec{E}_1 = \vec{E}_{01} + \vec{E}^{scar}(\vec{M}_s) + \vec{E}^{scar}(\vec{J}_1). \tag{2}$$

For the internal problem, as shown in Fig. 2 (b), the equivalent magnetic current density $\vec{M}_s$ and the unknown electric current $\vec{J}_2$ are selected so that the fields outside equivalent surface Ω_4 are zero and inside are equal to the radiation produced by $\vec{E}_{02}$ and the scattered fields $\vec{E}^{scar}(\vec{J}_2)$ and $\vec{E}^{scar}(-\vec{M}_s)$. These fields must satisfy the boundary condition (1), where,

$$\vec{E}_2 = \vec{E}_{02} + \vec{E}^{scar}(\vec{J}_2) + \vec{E}^{scar}(-\vec{M}_s). \tag{3}$$

An alternate formulation of the TD-EFIE is applied in this paper to describe unknown equivalent magnetic current sheet over the slot and the unknown electric currents at the probe and the antenna. This formulation is based on the equivalence principle in addition to enforce the following boundary conditions:

- The tangential magnetic fields are contentious through the slot aperture both inside and outside the cavity.
- The source is considered at the bottom of the probe inside the cavity.
- The source is considered at the center of the antenna outside the cavity.

Taking into account the interaction between the probe, the antenna and slot we obtain the following system:

$$\begin{cases} \left[\vec{E}_{01} + \vec{E}^{scar}(\vec{J}_1) + \vec{E}^{scar}(\vec{M}_s)\right]_{tan} = \vec{0} \ over\ \Omega_1 \\ \left[\vec{E}_{02} + \vec{E}^{scar}(\vec{J}_2) + \vec{E}^{scar}(-\vec{M}_s)\right]_{tan} = \vec{0} \ over\ \Omega_2 \\ \left[\vec{E}^{scar}(\vec{J}_1) + \vec{E}^{scar}(\vec{M}_s)\right]_{tan} \\ \qquad = \left[\vec{E}^{scar}(\vec{J}_2) + \vec{E}^{scar}(-\vec{M}_s)\right]_{tan} over\ \Omega_3 \\ \left[\vec{E}^{scar}(\vec{J}_1) + \vec{E}^{scar}(\vec{M}_s)\right]_{tan} = \vec{0} \ over\ \Omega_4 \\ \left[\vec{E}^{scar}(\vec{J}_2) + \vec{E}^{scar}(-\vec{M}_s)\right]_{tan} = \vec{0} \ over\ \Omega_4 \end{cases}, \tag{4}$$

where

$$\vec{E}^{scar}\left(\vec{M}_s\right) = -\frac{1}{\varepsilon}\nabla \times \vec{F}, \tag{5}$$

$$\vec{E}^{scar}(\vec{J}_i) = -\frac{\partial}{\partial t}\vec{A}_i - \nabla \varphi_i. \tag{6}$$

The magnetic vector and electric scalar potentials, $\vec{A}_i$ and φ_i, are expressed on the antenna (i=1) or the probe (i=2) which are mathematically given by:

$$\vec{A}_i(x,y,t) = \frac{\mu}{4\pi}\iint_{\Omega_i} \frac{\vec{J}_i(x',y',t-R_{ij}/C)}{R_{ij}(x,y,x',y')}\,ds',\ (x,y) \in \Omega_j, \tag{7}$$

$$\varphi_i(x,y,t) = \frac{1}{4\pi\varepsilon}\iint_{\Omega_i} \frac{q_i(x',y',t-R_{ij}/C)}{R_{ij}(x,y,x',y')}\,ds',\ (x,y) \in \Omega_j, \tag{8}$$

where μ is the permeability and C is the velocity of propagation of the electromagnetic wave in free space.

The potential electric vector $\vec{F}$ is given by the time retarded integral equation involving the magnetic current $\vec{M}_s$. It is mathematically obtained by application of the concept of electromagnetic duality for Maxwell theories:

$$\vec{F}(x,y,t) = \frac{\varepsilon}{4\pi}\iint_{\Omega_3} \frac{\vec{M}_s(x',y',t-R_{3j}/C)}{R_{3j}(x,y,x',y')}\,ds',\ (x,y) \in \Omega_j, \tag{9}$$

where $\vec{M}_s$ is the equivalent density current vector along Ω_3 and ε is permittivity of free space. The retarded time is expressed by $t - R_{ij}/C$. The distance $R_{ij} = \sqrt{(x-x')^2 + (y-y')^2}$ represents the interaction between the observation point $(x,y) \in \Omega_j$ and the source point $(x',y') \in \Omega_i$, as shown in Fig. 4.

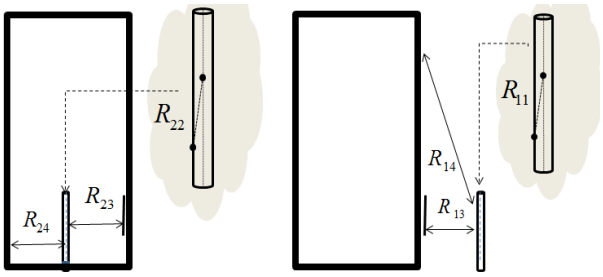

Fig. 4. The different distances between the observation and source points for the internal and external equivalent problems.

For convenience of numerical computation [13], it is useful to derive the scalar and vector potentials from the sources terms by means of the Hertz vectors which does not have a time integral term. Hence, the electric current and the charge density can be expressed in terms of the single Hertz vector $\vec{G}_i$:

$$\vec{J}_i(x,y,t) = \frac{d}{dt}\vec{G}_i(x,y,t), \tag{10}$$

$$q_i(x,y,t) = -\nabla.\vec{G}_i(x,y,t). \tag{11}$$

The magnetic current is also expressed by means of the Hertz vector $\vec{L}$:

$$M_s(x,y,t) = \frac{d}{dt}\vec{L}(x,y,t). \tag{12}$$

By substituting (5)-(12) in (4), we obtain the following time domain integral equations system:

$$\left[\begin{array}{l} -\frac{\mu}{4\pi}\frac{\partial^2}{\partial t^2}\iint_{\Omega_1}\frac{\vec{G}_1(x',y',t-R_{11}/C)}{R_{11}(x,y,x',y')}ds' \\ +\frac{1}{4\pi\varepsilon}\nabla\iint_{\Omega_1}\frac{\nabla.\vec{G}_1(x',y',t-R_{11}/C)}{R_{11}(x,y,x',y')} \\ -\frac{1}{4\pi}\nabla\times\iint_{\Omega_3}\frac{1}{R_{31}(x,y,x',y')}\frac{d}{dt}\vec{L}(x',y',t-R_{31}/C)ds' \end{array}\right] = -\vec{E}_{01}(x,y,t) \quad (13)$$

$$\left[\begin{array}{l} -\frac{\mu}{4\pi}\frac{\partial^2}{\partial t^2}\iint_{\Omega_2}\frac{\vec{G}_2(x',y',t-R_{22}/C)}{R_{22}(x,y,x',y')}ds' \\ +\frac{1}{4\pi\varepsilon}\nabla\iint_{\Omega_2}\frac{\nabla.\vec{G}_2(x',y',t-R_{22}/C)}{R_{22}(x,y,x',y')} \\ +\frac{1}{4\pi}\nabla\times\iint_{\Omega_3}\frac{1}{R_{32}(x,y,x',y')}\frac{d}{dt}\vec{L}(x',y',t-R_{32}/C)ds' \end{array}\right] = -\vec{E}_{02}(x,y,t) \quad (14)$$

$$\left[\begin{array}{l} -\frac{\mu}{4\pi}\frac{\partial^2}{\partial t^2}\iint_{\Omega_1}\frac{\vec{G}_1(x',y',t-R_{13}/C)}{R_{13}(x,y,x',y')}ds' \\ +\frac{1}{4\pi\varepsilon}\nabla\iint_{\Omega_1}\frac{\nabla.\vec{G}_1(x',y',t-R_{13}/C)}{R_{13}(x,y,x',y')} \\ -\frac{1}{4\pi}\nabla\times\iint_{\Omega_3}\frac{1}{R_{33}(x,y,x',y')}\frac{d}{dt}\vec{L}(x',y',t-R_{33}/C)ds' \end{array}\right]$$

$$= \left[\begin{array}{l} -\frac{\mu}{4\pi}\frac{\partial^2}{\partial t^2}\iint_{\Omega_2}\frac{\vec{G}_2(x',y',t-R_{23}/C)}{R_{23}(x,y,x',y')}ds' \\ +\frac{1}{4\pi\varepsilon}\nabla\iint_{\Omega_2}\frac{\nabla.\vec{G}_2(x',y',t-R_{23}/C)}{R_{23}(x,y,x',y')} \\ +\frac{1}{4\pi}\nabla\times\iint_{\Omega_3}\frac{1}{R_{33}(x,y,x',y')}\frac{d}{dt}\vec{L}(x',y',t-R_{33}/C)ds' \end{array}\right], \quad (15)$$

$$\left[\begin{array}{l} -\frac{\mu}{4\pi}\frac{\partial^2}{\partial t^2}\iint_{\Omega_1}\frac{\vec{G}_1(x',y',t-R_{14}/C)}{R_{14}(x,y,x',y')}ds' \\ +\frac{1}{4\pi\varepsilon}\nabla\iint_{\Omega_1}\frac{\nabla.\vec{G}_1(x',y',t-R_{14}/C)}{R_{14}(x,y,x',y')} \\ -\frac{1}{4\pi}\nabla\times\iint_{\Omega_3}\frac{1}{R_{34}(x,y,x',y')}\frac{d}{dt}\vec{L}(x',y',t-R_{34}/C)ds' \end{array}\right] = \vec{0}, \quad (16)$$

$$\left[\begin{array}{l} -\frac{\mu}{4\pi}\frac{\partial^2}{\partial t^2}\iint_{\Omega_2}\frac{\vec{G}_2(x',y',t-R_{24}/C)}{R_{24}(x,y,x',y')}ds' \\ +\frac{1}{4\pi\varepsilon}\nabla\iint_{\Omega_2}\frac{\nabla.\vec{G}_2(y',t-R_{24}/C)}{R_{24}(x,y,x',y')} \\ +\frac{1}{4\pi}\nabla\times\iint_{\Omega_3}\frac{1}{R_{34}(x,y,x',y')}\frac{d}{dt}\vec{L}(x',y',t-R_{34}/C)ds' \end{array}\right] = \vec{0}. \quad (17)$$

The TD-EFIE are solved in space and time domains by applying the Method of Moments (MoM) [12]. Firstly, the problem is converted to a discrete one by employing a system of appropriate space-time bases functions. Secondly, a testing procedure is applied to convert the discrete vector functional equation into a linear scalar system of equations.

We start the space numerical procedure by the choice of suitable space basis functions in order to approximate the unknown Hertz vectors $\vec{G}_1$, $\vec{G}_2$ and $\vec{L}$. Indeed, the choice of the basis function strongly influences the properties of the MoM approximation of the unknowns. We define the spatial basis functions as the piecewise triangular functions [13] associated with Dirac function $\vec{f}_n = H_n^{(\Omega_i)}.\Lambda_{\chi_j}^{(\Omega_i)}\vec{u}$, where,

$$H_k^{(\Omega_i)}(h) = \begin{cases} \frac{h-h_{k-1}}{h_k-h_{k-1}}, & h\in[h_{k-1},h_k] \\ \frac{h_{k+1}-h}{h_{k+1}-h_k}, & h\in[h_k,h_{k+1}] \\ 0 \quad , & otherwise \end{cases}. \quad (18)$$

$$\Lambda_{\chi_j}^{(\Omega_i)}(\chi) = \begin{cases} 1, & \chi=\chi_j \\ 0, & otherwise \end{cases}$$

The choice of the piecewise triangular function has the following advantages: it minimized the required computational and it leads to an accurate evaluation of the unknowns with few expansion functions.

The goal of the association between the Dirac function and the piecewise triangular function is metalized the domains Ω_i only.

Now, we express the Hertz vectors $\vec{G}_i$ and $\vec{L}$ in terms of vector basis functions $\vec{f}_n$ and $\vec{h}_n = \vec{n}\times\vec{f}_n$, respectively:

$$\left[\begin{array}{l} \vec{G}_1(x,y,t) = \sum_{n=1}^{N_1} g_n^1(t)\vec{f}_n^{\,1}(x,y) \\ \vec{f}_n^{\,1}(x,y) = H_n^{(\Omega_1)}(y).\Lambda_{x_A}^{(\Omega_1)}(x)\vec{y} \end{array}\right., \quad (19)$$

$$\left[\begin{array}{l} \vec{G}_2(x,y,t) = \sum_{n=1}^{N_2} g_n^2(t)\vec{f}_n^{\,2}(x,y) \\ \vec{f}_n^{\,2}(x,y) = H_n^{(\Omega_{21})}(y).\Lambda_{x_p}^{(\Omega_2)}(x)\vec{y} \end{array}\right., \quad (20)$$

$$\left[\begin{array}{l} \vec{L}(x,y,t) = \sum_{n=1}^{N_3} l_n(t)\vec{h}_n(x,y) \\ \vec{h}_n = \vec{n}\times\vec{f}_n \\ \vec{f}_n(x,y) = H_n^{(\Omega_3)}(y).\Lambda_{x_S}^{(\Omega_3)}(x)\vec{y} \end{array}\right. . \quad (21)$$

Note that the axis of the antenna, the probe and the slot are divided into N_1, N_2 and N_3 equal sub-domains of which the space step is Δy.

In order to discretize Ω_4, we divide the cavity walls in $N_4 = N_{4x}\times N_{4y}$ equal sub-domains whose the lengths are Δx and Δy along x-y directions, respectively. The functions $\vec{f}_n^{\,4}$ illustrated in Fig. 5 is given by:

$$\left\{\begin{array}{l} f_{n,y}^4(x,y) = H_n^{(\Omega_4)}(y).\Lambda_{x_{\{1,N_{4x}\}}}^{(\Omega_4)}(x) \\ f_{n,x}^4(x,y) = H_{\{1,N_{4y}\}}^{(\Omega_4)}(y).\Lambda_{x_n}^{(\Omega_4)}(x) \end{array}\right. . \quad (22)$$

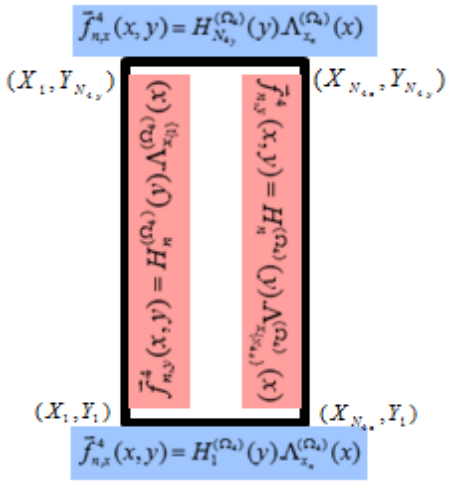

Fig. 5. Testing function $\vec{f}_n^{\,4}$.

We substitute (19)-(21) into (13)-(17), then we apply the spatial testing procedure, we obtain:

$$\left[\begin{array}{l}\sum_{n=1}^{N_1}\left[-\mu a_{mn}^{11}\frac{d^2 g_n^1(t-R_{mn}^{11}/C)}{dt^2}+\frac{b_{mn}^{11}}{\varepsilon}g_n^1(t-R_{mn}^{11}/C)\right]\\ +\sum_{n=1}^{N_3}-c_{mn}^{31}\frac{dI_n(t-R_{mn}^{31}/C)}{dt}\end{array}\right]=-E_m^1(t)\quad,(23)$$

$$\left[\begin{array}{l}\sum_{n=1}^{N_2}\left[-\mu a_{mn}^{22}\frac{d^2 g_n^2(t-R_{mn}^{22}/C)}{dt^2}+\frac{b_{mn}^{22}}{\varepsilon}g_n^2(t-R_{mn}^{22}/C)\right]\\ +\sum_{n=1}^{N_3}c_{mn}^{32}\frac{dI_n(t-R_{mn}^{32}/C)}{dt}\end{array}\right]=-E_m^2(t)\quad,(24)$$

$$\left[\begin{array}{l}\sum_{n=1}^{N_1}\left[-\mu a_{mn}^{13}\frac{d^2 g_n^1(t-R_{mn}^{13}/C)}{dt^2}+\frac{b_{mn}^{13}}{\varepsilon}g_n^1(t-R_{mn}^{13}/C)\right]\\ -\sum_{n=1}^{N_2}\left[-\mu a_{mn}^{23}\frac{d^2 g_n^2(t-R_{mn}^{23}/C)}{dt^2}+\frac{b_{mn}^{23}}{\varepsilon}g_n^2(t-R_{mn}^{23}/C)\right]\\ +2\sum_{n=1}^{N_3}-c_{mn}^{33}\frac{dI_n(t-R_{mn}^{33}/C)}{dt}\end{array}\right]=0\quad,(25)$$

$$\left[\begin{array}{l}\sum_{n=1}^{N_1}\left[-\mu a_{mn}^{14}\frac{d^2 g_n^1(t-R_{mn}^{14}/C)}{dt^2}+\frac{b_{mn}^{14}}{\varepsilon}g_n^1(t-R_{mn}^{14}/C)\right]\\ +\sum_{n=1}^{N_3}-c_{mn}^{34}\frac{dI_n(t-R_{mn}^{34}/C)}{dt}\end{array}\right]=0\quad,(26)$$

$$\left[\begin{array}{l}\sum_{n=1}^{N_2}\left[-\mu a_{mn}^{24}\frac{d^2 g_n^2(t-R_{mn}^{24}/C)}{dt^2}+\frac{b_{mn}^{24}}{\varepsilon}g_n^2(t-R_{mn}^{24}/C)\right]\\ +\sum_{n=1}^{N_3}c_{mn}^{34}\frac{dI_n(t-R_{mn}^{34}/C)}{dt}\end{array}\right]=0\quad.(27)$$

We assume that the unknown transient quantities $\{g_n^i, I_n\}$ does not change appreciably within the segment Δy so that $\tau^{ij}=t-R^{ij}/C\rightarrow\tau_{mn}^{ij}=t-R_{mn}^{ij}/C$:

$$\begin{aligned}E_m^j(t)&=\left\langle \vec{f}_m^{\,j}(x,y),\vec{n}\times\vec{E}_{0j}(x,y,t)\right\rangle\\&=\iint_{\Omega_j}\vec{f}_m^{\,j}(x,y).\left[\vec{n}\times\vec{E}_{0j}(x,y,t)\right]ds\end{aligned},\quad(28)$$

$$\begin{cases}a_{mn}^{ij}=\left\langle f_m^j(x,y),\frac{1}{4\pi}\iint_{\Omega_i}\frac{f_n^i(x',y')}{R_{ij}(x,y,x',y')}ds\right\rangle\\ b_{mn}^{ij}=\left\langle f_m^j(x,y),\frac{1}{4\pi}\nabla\iint_{\Omega_i}\frac{\nabla f_n^i(x',y')}{R_{ij}(x,y,x',y')}\right\rangle\\ c_{mn}^{3j}=\left\langle f_m^j(x,y),\frac{1}{4\pi}\nabla\times\iint_{\Omega_3}\frac{\vec{h}_m(x',y')}{R_{3j}(x,y,x',y')}ds'\right\rangle\end{cases}.\quad(29)$$

On the other hand, we consider the temporal procedure. In order to obtain stable and accurate solutions, a temporal basis functions derived from the Laguerre polynomials [14] is applied. The transient electric and magnetic coefficients introduced in (19) and (20) are expanded by:

$$g_n^i(t)\approx\sum_{a=0}^{\infty}g_{n,a}^i\varphi_a(st),\quad(30)$$

$$I_n(t)\approx\sum_{a=0}^{\infty}I_{n,a}\varphi_a(st),\quad(31)$$

where $\{g_{n,a}^i, I_{n,a}\}$ are the unknown coefficients; $\{\varphi_a(st), a=0..\infty\}$ is the temporal basis functions derived from the Laguerre function $\left(\varphi_a(st)=e^{-st/2}L_a(st)\right)$. So, the term $L_a(st)$ represents the Laguerre polynomial of order "a" and "s" is a time scaling factor [17]. The mathematical properties of these functions, the first and the second derivatives are introduced in [14]-[15].

In order to apply the Galerkin's Method [12] in time domain, we substitute (30)-(33) into (23)-(27) and we apply the temporal testing procedure with $\varphi_b(st)$, we obtain the following system:

$$\left\{\begin{array}{l}\left[\begin{array}{l}\sum_{n=1}^{N_1}\left[-s^2\mu a_{mn}^{11}\sum_{a=0}^{b}\left[\frac{1}{4}g_{n,a}^1+\sum_{k=0}^{a-1}(a-k)g_{n,k}^1\right]I_{ba}\left(s\left(R_{mn}^{11}/C\right)\right)+\frac{b_{mn}^{11}}{\varepsilon}\sum_{a=0}^{b}g_{n,a}^1I_{ba}\left(s\left(R_{mn}^{11}/C\right)\right)\right]\\ +\sum_{n=1}^{N_3}-sc_{mn}^{31}\sum_{a=0}^{b}\left[\frac{1}{2}I_{n,a}+\sum_{k=0}^{a-1}I_{n,k}\right]I_{ba}\left(s\left(R_{mn}^{31}/C\right)\right)\end{array}\right]=-E_{m,b}^1(t)\\ \left[\begin{array}{l}\sum_{n=1}^{N_2}\left[-s^2\mu a_{mn}^{22}\sum_{a=0}^{b}\left[\frac{1}{4}g_{n,a}^2+\sum_{k=0}^{a-1}(a-k)g_{n,k}^2\right]I_{ba}\left(s\left(R_{mn}^{22}/C\right)\right)+\frac{b_{mn}^{22}}{\varepsilon}\sum_{a=0}^{b}g_{n,a}^2I_{ba}\left(s\left(R_{mn}^{22}/C\right)\right)\right]\\ +\sum_{n=1}^{N_3}sc_{mn}^{32}\sum_{a=0}^{b}\left[\frac{1}{2}I_{n,a}+\sum_{k=0}^{a-1}I_{n,k}\right]I_{ba}\left(s\left(R_{mn}^{32}/C\right)\right)\end{array}\right]=-E_{m,b}^2(t)\\ \left[\begin{array}{l}\left[\sum_{n=1}^{N_1}\left[-s^2\mu a_{mn}^{13}\sum_{a=0}^{b}\left[\frac{1}{4}g_{n,a}^1+\sum_{k=0}^{a-1}(a-k)g_{n,k}^1\right]I_{ba}\left(s\left(R_{mn}^{13}/C\right)\right)+\frac{b_{mn}^{13}}{\varepsilon}\sum_{a=0}^{b}g_{n,a}^1I_{ba}\left(s\left(R_{mn}^{13}/C\right)\right)\right]\right]\\ \left[-\sum_{n=1}^{N_2}\left[-s^2\mu a_{mn}^{23}\sum_{a=0}^{b}\left[\frac{1}{4}g_{n,a}^2+\sum_{k=0}^{a-1}(a-k)g_{n,k}^2\right]I_{ba}\left(s\left(R_{mn}^{23}/C\right)\right)+\frac{b_{mn}^{23}}{\varepsilon}\sum_{a=0}^{b}g_{n,ab}^2I_{ba}\left(s\left(R_{mn}^{23}/C\right)\right)\right]\right]\\ \left[+2\sum_{n=1}^{N_3}-sc_{mn}^{33}\sum_{a=0}^{b}\left[\frac{1}{2}I_{n,a}+\sum_{k=0}^{a-1}I_{n,k}\right]I_{ba}\left(s\left(R_{mn}^{23}/C\right)\right)\right]\end{array}\right]=0\\ \left[\begin{array}{l}\sum_{n=1}^{N_1}\left[-s^2\mu a_{mn}^{14}\sum_{a=0}^{b}\left[\frac{1}{4}g_{n,a}^1+\sum_{k=0}^{a-1}(a-k)g_{n,k}^1\right]I_{ba}\left(s\left(R_{mn}^{14}/C\right)\right)+\frac{b_{mn}^{14}}{\varepsilon}\sum_{a=0}^{b}g_{n,a}^1I_{ba}\left(s\left(R_{mn}^{14}/C\right)\right)\right]\\ +\sum_{n=1}^{N_3}-sc_{mn}^{34}\sum_{a=0}^{b}\left[\frac{1}{2}I_{n,a}+\sum_{k=0}^{a-1}I_{n,k}\right]I_{ba}\left(s\left(R_{mn}^{24}/C\right)\right)\end{array}\right]=0\\ \left[\begin{array}{l}\sum_{n=1}^{N_2}\left[-s^2\mu a_{mn}^{24}\sum_{a=0}^{b}\left[\frac{1}{4}g_{n,a}^2+\sum_{k=0}^{a-1}(a-k)g_{n,k}^2\right]I_{ba}\left(s\left(R_{mn}^{24}/C\right)\right)+\frac{b_{mn}^{24}}{\varepsilon}\sum_{a=0}^{b}g_{n,a}^2I_{ba}\left(s\left(R_{mn}^{24}/C\right)\right)\right]\\ +\sum_{n=1}^{N_3}sc_{mn}^{34}\sum_{a=0}^{b}\left[\frac{1}{2}I_{n,a}+\sum_{k=0}^{a-1}I_{n,k}\right]I_{ba}\left(s\left(R_{mn}^{34}/C\right)\right)\end{array}\right]=0\end{array}\right.\quad.(32)$$

We note that, we can change the upper limit of the sum (30) and (31) form ∞ to "b" based on the orthogonality condition detailed in [14]:

$$I_{ba}(s\frac{R_{mn}^{ij}}{C}) = \left\langle \varphi_b(st), \varphi_a(s(t-\frac{R_{mn}^{ij}}{C})) \right\rangle = \int_0^{\infty} \varphi_b(st)\varphi_a(s(t-\frac{R_{mn}^{ij}}{C}))d(st) = \begin{cases} e^{-\frac{sR_{mn}}{2C}}\left[L_{b-a}(s\frac{R_{mn}}{C}) - L_{b-a-1}(s\frac{R_{mn}}{C}) \right], & a \le b \\ 0, & a > b \end{cases}.$$

The scalar product of the field E_m^v (28) by the Laguerre function of order « b » is given by:

$$E_{b,m}^v = \int_0^{\infty} \varphi_b(st) E_m^v(t) d(st). \quad (33)$$

In the system (32), we move the terms including $g_{n,b}^1$, $g_{n,b}^2$ and $l_{n,b}$, which is known for a<b to the right-hand side. Rewriting the resulting equations in a simple form, we have:

$$\sum_{n=1}^{N_1} A_{mn}^{11} g_{n,b}^1 + \sum_{n=1}^{N_3} B_{mn}^{31} l_{n,b} = E_{m,b}^1 + S_{m,b}^1, \quad (34)$$

$$\sum_{n=1}^{N_2} A_{mn}^{22} g_{n,b}^2 + \sum_{n=1}^{N_3} B_{mn}^{32} l_{n,b} = E_{m,b}^2 + S_{m,b}^2, \quad (35)$$

$$\sum_{n=1}^{N_1} A_{mn}^{13} g_{n,b}^1 + \sum_{n=1}^{N_2} A_{mn}^{23} g_{n,b}^2 + \sum_{n=1}^{N_3} B_{mn}^{33} l_{n,b} = S_{m,b}^3, \quad (36)$$

$$\sum_{n=1}^{N_1} A_{mn}^{14} g_{n,b}^1 + \sum_{n=1}^{N_3} B_{mn}^{34} l_{n,b} = K_{m,b}^4, \quad (37)$$

$$\sum_{n=1}^{N_2} A_{mn}^{24} g_{n,b}^2 + \sum_{n=1}^{N_3} B_{mn}^{34} l_{n,b} = H_{m,b}^4. \quad (38)$$

The spatial matrices (A^{ij}, B^{ij}) and the retarded terms $S_{m,b}^1$, $S_{m,b}^2$, $S_{m,b}^3$, $K_{m,b}^4$ and $H_{m,b}^4$ are presented in appendix.

Now, we write (34)-(38) in a matrix form:

$$\begin{bmatrix} [A^{11}] & [0] & [B^{31}] \\ [0] & [A^{22}] & [B^{32}] \\ [A^{13}] & [A^{23}] & [B^{33}] \\ [A^{14}] & [0] & [B^{34}] \\ [0] & [A^{24}] & [B^{34}] \end{bmatrix} \begin{bmatrix} g_b^1 \\ g_b^2 \\ l_b \end{bmatrix} = \begin{bmatrix} E_b^1 + S_b^1 \\ E_b^2 + S_b^2 \\ S_b^3 \\ K_b^4 \\ H_b^4 \end{bmatrix} \Leftrightarrow A^* X = B. \quad (39)$$

It is important to note that the matrix A is not a function of the degree of the temporal testing function "b". Therefore, we obtain the unknown coefficients by solving (39) as increasing the degree of temporal testing functions. Consequently, we solve the problem only in space for each degree of the Laguerre function. Finally, the transient currents are calculated by:

$$J_i^j(t) = \frac{d}{dt} G_i^j(t) = s\sum_{a=0}^{A}\left[\frac{1}{2} g_{i,a}^j + \sum_{k=0}^{a-1} g_{i,k}^j \right] \varphi_a(st), \quad (40)$$

$$M_i(t) = \frac{d}{dt} L_i(t) = s\sum_{a=0}^{A}\left[\frac{1}{2} l_{i,a} + \sum_{k=0}^{a-1} l_{i,k} \right] \varphi_a(st), \quad (41)$$

where A is the maximum order of the Laguerre function [16].

III. NUMERICAL RESULTS

In this section, we present the different numerical results by applying the proposed formulation and we compared the latters with the results obtained by the B-Spline scheme, developed in [22]. Thus, we consider the structure shown in Fig. 6. Their related parameters are presented in Table 1. The space parameters N_i, $1 \le i \le 4$ are described in Table 2.

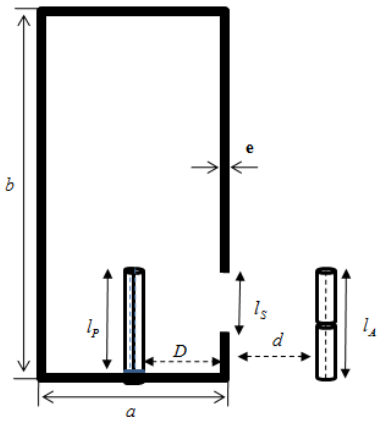

Fig. 6. Structure of the problem.

Table 1: Cavity parameters

Symbol	Quantity	Value
a	Cavity width	0.346λ m
b	Cavity length	0.692λ m
l_s	Slot length	0.048λ m
(x_s,y_s)	Center of slot	(0.346λ, 0.173λ)
l_P	Probe length	0.25λ m
(x_p,y_p)	Probe center	(0.172λ, 0)
l_A	Antenna length	0.25λ m
(x_A,y_A)	Position of antenna	(a+0. 172λ,0)
e	Thickness	10^{-5}

In this table, we used same parameters of the cavity presented in [2] at the resonance frequency of 1.9 GHz.

Table 2: Space parameters

Symbol	Quantity	Value
Δx	Space step	2.73 10^{-4} m
Δy	Space step	5.46 10^{-4} m
N_1	Number of antenna sub-domains	$l_A/\Delta y$
N_2	Number of probe sub-domains	$L_p/\Delta y$
N_3	Number of slot sub-domains	$L_s/\Delta y$
N_4	Number of cavity walls sub-domains	$(N_{4x},N_{4y})=(a/\Delta x,b/\Delta y)$

We assume that the probe (inside the cavity) is excited by the Gaussian pulse voltage generator $V(t)$ at the bottom. The antenna is also excited by $V(t)$ at its center. The source $V(t)$ is expressed by:

$$V(t) = V_0 e^{\left(-g^2(t-t_0)\right)}, \quad (42)$$

with parameters $V_0 = 1V$, $g = 10^8 s^{-1}$ and $t_0 = 10^{-8} s$. We suppose that the antenna and the probe have same length $\left(l_A = l_p\right)$ and same radius e.

The value of the time scale factor s is 2.10^9 and the number of Laguerre functions A is fixed at 80. The values of s and A are sufficient to get accurate solutions. In fact, the terms s and A are the Laguerre function parameters.

In order to verify the results, we apply the B-Spline scheme developed in [22]. In fact, for the two schemes (Laguerre and B-Spline), we consider the case when the two antennas are excited by (42). The transient responses of the structure are depicted in Fig. 7 and Fig. 8. Thus, we clearly observe the good agreement between the results obtained by the two schemes.

Consequently, we apply the Laguerre scheme developed in this paper to study the coupling between the components of the designed communication system. This scheme is unconditionally stable. The space and the time steps are not related as the most temporal techniques (FDTD, TLM, MOT). We obtain stable and accurate solutions.

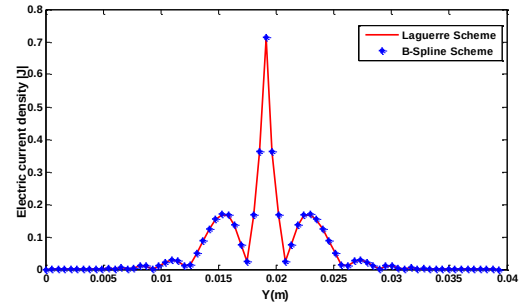

(a)

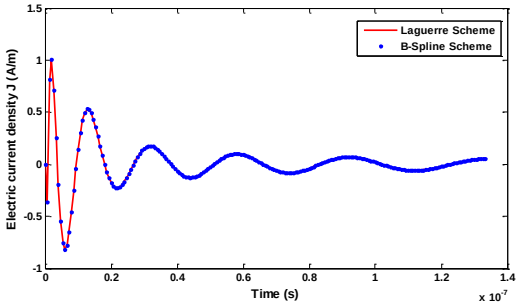

(b)

Fig. 7. The transient response of the antenna: (a) the normalized electric current density at the instant t=1.33*10^{-9} s, and (b) transient electric current density at the center of antenna.

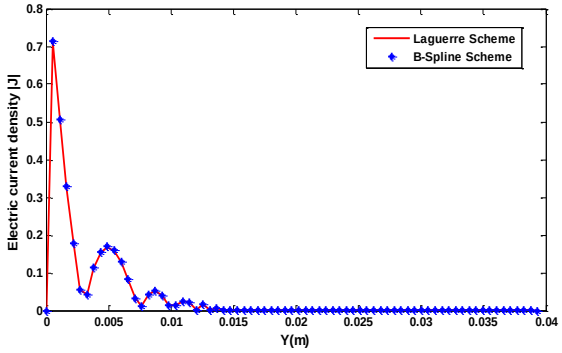

(a)

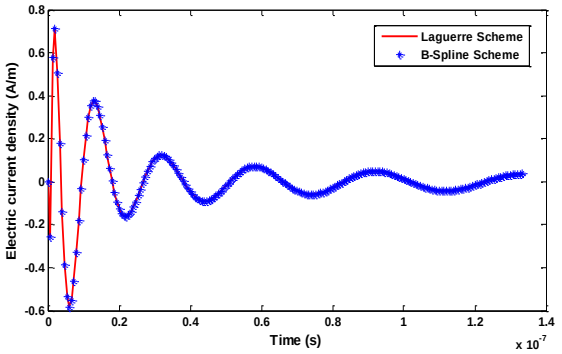

(b)

Fig. 8. The transient response of the probe: (a) the normalized electric current density at the instant t=1.33*10^{-9} s, and (b) transient electric current density at the top of the probe.

A. Electric and magnetic currents distributions

In order to describe the transient behaviors of the structure, three cases are considered:

- The antenna and the probe are both excited.
- Only the antenna is excited.
- Only the probe is excited.

The transient responses are determined at the center of antenna, at the bottom of probe and the center of slot.

Figure 9 shows the space distribution of electric current density of the antenna. It is obvious that the peak of the electric current occurred at the center point as expected for the case when the antenna is excited. But when the antenna is unexcited, the current vanish. The transient response plotted, in Fig. 10, at the center of the antenna confirms the latter interpretation.

The transient response of the probe is shown in Fig. 11 and Fig. 12; we should note that the peak of electric current occurred at the feed point and the amplitude vanish when the probe is unexcited. The miniature curve in Fig. 11 presents the coupling effect when the probe is unexcited and the antenna is excited.

The magnetic current density is presented in space and time when the antenna and the probe are both excited in Fig. 13.

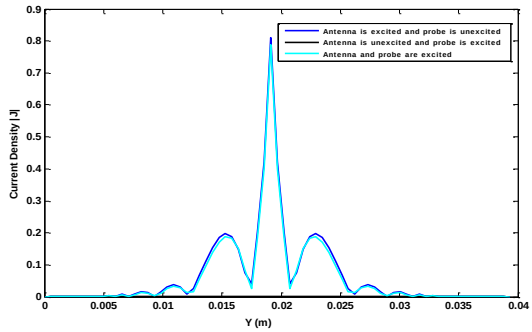

Fig. 9. The normalized electric current density of the antenna at the instant t=1.33*10^{-9} s.

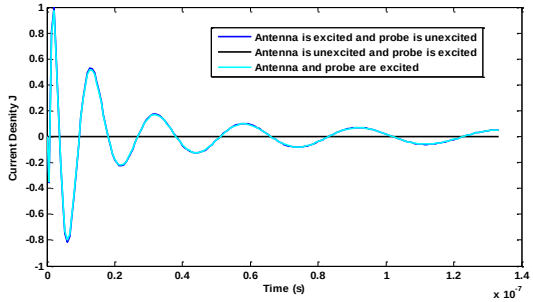

Fig. 10. Transient electric current density at the center of antenna.

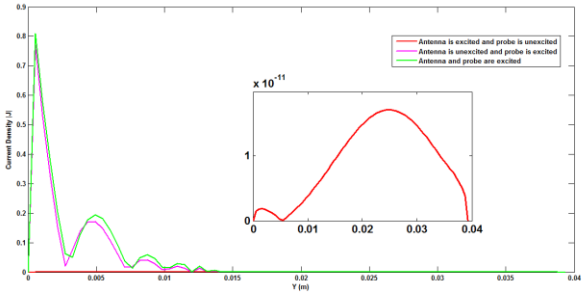

Fig. 11. The normalized electric current density of the probe at the instant t=1.33*10^{-9} s.

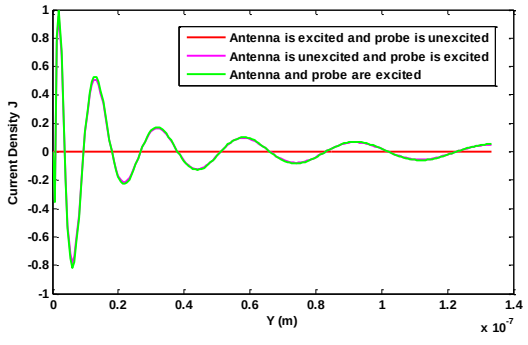

Fig. 12. Transient electric current density at the top of the probe.

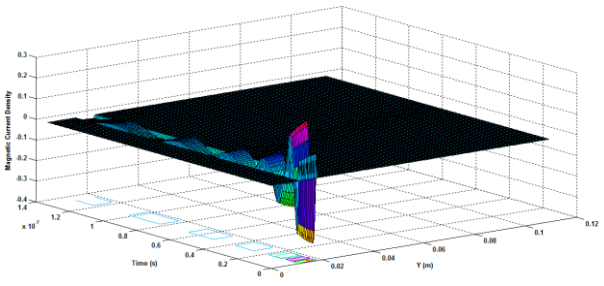

Fig. 13. The normalized magnetic current density at the slot when the antenna and the probe are excited.

B. Study of coupling through the slot depending on separate distances d and D

In order to study the Antenna-Slot coupling and Probe-Slot coupling, we consider four separate distances:

$$d = D = d_1 = 0.018\times \mathrm{a}, \quad d = D = d_2 = 0.146\times \mathrm{a},$$

$$d = D = d_3 = 0.274\times \mathrm{a}, \quad d = D = d_4 = 0.875\times \mathrm{a}.$$

Starting by the study of the coupling effect of antenna and cavity as function of different distances d (the value of D is fixed in Table 1).

Figure 14 represents the theoretical coupling between the antenna and the slot calculated via the matrix Aij. It is clearly that the coupling vanish from $d_c = 0.005\,\mathrm{m}$. The transient magnetic current plotted in Fig. 15 for different separated distances d confirms the theoretical results. We note that, if $d > d_c$, the magnetic current does not change.

To study the coupling between the cavity and the probe, we vary the separate distances D and we fix the distance d (Table 1).

The coupling vanishes from $d_c = 0.008\,\mathrm{m}$ as presented in Fig. 16. This result is detailed in Fig. 17; but for the distance d_4, the current amplitude is non-zero and a low variation is detected. This variation is due to the effect of the cavity walls which amplified the currents inside the cavity.

Also, lower values of the electric current at the probe and the magnetic current at the slot are observed when the cavity size becomes larger (Fig. 18).

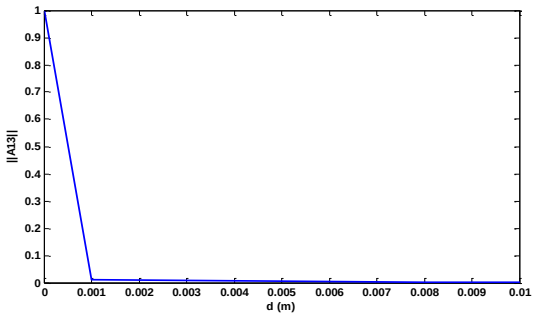

Fig. 14. Matrix coupling antenna-slot.

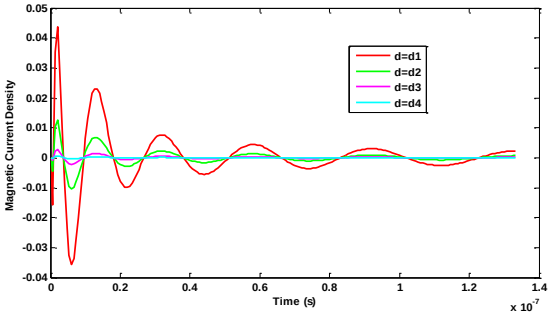

Fig. 15. Transient magnetic current at the center of the slot for various distances d.

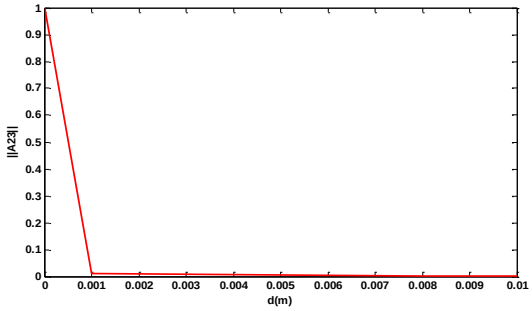

Fig. 16. Matrix coupling between probe-slot.

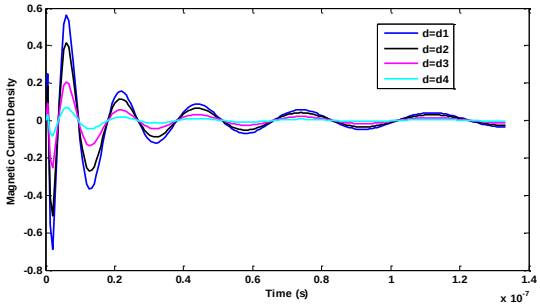

Fig. 17. Transient magnetic current at the center of the slot for various distances D.

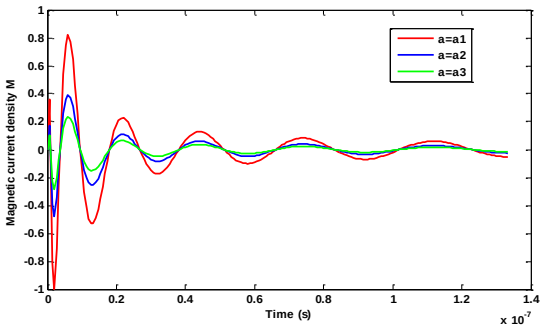

Fig. 18. Transient magnetic current at the center of slot for various cavity widths a=a1=0.55*λ, a=a2=0.69*λ and a=a3=0.75*λ.

C. Study of coupling through the slot depending on slot length

It is very important to study the coupling taking into account the length of the slot. Therefore, we vary the latter parameter and two cases can be defined. One hand, when only the probe is excited, the transient current density at the top of the antenna as shown in Fig. 19. The amplitude becomes more important when the length of the slot is increased. This result is confirmed by this shown in Fig. 10.

On the other hand, when only the antenna is excited, the transient current density at the top of probe for the shorter slot is lower than the longer ones, as depicted in Fig. 20.

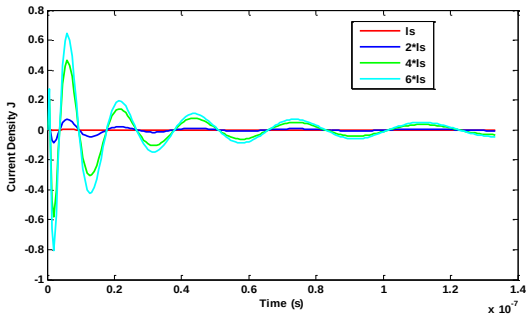

Fig. 19. Transient current at the top of the antenna when the probe is excited and for various lengths of slot.

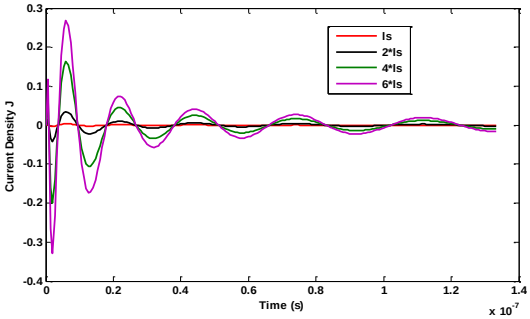

Fig. 20. Transient current at the top of the probe when the antenna is excited and for various lengths of slot.

IV. CONCLUSIONS

The transient behaviors of communication system composed on rectangular cavity containing an interior scatterer coupled to an external scatterer through a slot were studied. A 2-D numerical time domain formulation based on the combination of the equivalence principle and the MoM has been successfully developed and applied to the designed system.

The physical coupling effects between the components of the system through the slot have been provided depending on the separate distances and the lengths of the slot. Stable and accurate results have been found mainly with electric and magnetic currents

responses.

This formulation can be extended to 3-D and applied for many complex structures.

APPENDIX

The spatial matrices A_{mn}^{ij} and B_{mn}^{ij} can be defined as:

$$A_{mn}^{ij} = \left[-s^2 \frac{\mu a_{mn}^{ij}}{4} + \frac{b_{mn}^{ij}}{\varepsilon} \right] I_{bb}\left(s\left(R_{mn}^{ij}/C\right)\right),$$

$$B_{mn}^{ij} = \pm s \frac{c_{mn}^{ij}}{2} I_{bb}\left(s\left(R_{mn}^{ij}/C\right)\right),$$

where

$$I_{bb}\left(s\left(R_{mn}^{ij}/C\right)\right) = e^{-\frac{s}{2}\left(R_{mn}^{ij}/C\right)}.$$

The retarded terms takes the following forms:

$$S_{m,b}^{1} = -\begin{bmatrix} -s^2\mu\sum_{n=1}^{N_1} a_{mn}^{11}\sum_{k=0}^{b-1}(b-k)g_{n,k}^{1} I_{bb}(s(R_{mn}^{11}/C)) \\ -s^2\mu\sum_{n=1}^{N_1} a_{mn}^{11}\sum_{a=0}^{b-1}\left[\frac{1}{4}g_{n,a}^{1} + \sum_{k=0}^{a-1}(a-k)g_{n,k}^{1}\right] I_{ba}(s(R_{mn}^{11}/C)) \\ +\frac{1}{\varepsilon}\sum_{n=1}^{N_1} b_{mn}^{11}\sum_{a=0}^{b-1} g_{n,a}^{1} I_{ba}(s(R_{mn}^{11}/C)) \\ -\sum_{n=1}^{N_3} sc_{mn}^{13}\sum_{k=0}^{b-1} l_{n,k} I_{bb}(s(R_{mn}^{13}/C)) \\ -\sum_{n=1}^{N_3} sc_{mn}^{13}\sum_{a=0}^{b-1}\left[\frac{1}{2}l_{n,a} + \sum_{k=0}^{a-1} l_{n,k}\right] I_{ba}(s(R_{mn}^{13}/C)) \end{bmatrix},$$

$$S_{m,b}^{2} = -\begin{bmatrix} -s^2\mu\sum_{n=1}^{N_2} a_{mn}^{22}\sum_{k=0}^{b-1}(b-k)g_{n,k}^{2} I_{bb}(s(R_{mn}^{22}/C)) \\ -s^2\mu\sum_{n=1}^{N_2} a_{mn}^{22}\sum_{a=0}^{b-1}\left[\frac{1}{4}g_{n,a}^{2} + \sum_{k=0}^{a-1}(a-k)g_{n,k}^{2}\right] I_{ba}(s(R_{mn}^{22}/C)) \\ +\frac{1}{\varepsilon}\sum_{n=1}^{N_2} b_{mn}^{22}\sum_{a=0}^{b-1} g_{n,a}^{2} I_{ba}(s(R_{mn}^{22}/C)) \\ +\sum_{n=1}^{N_3} sc_{mn}^{23}\sum_{k=0}^{b-1} l_{n,k} I_{bb}(s(R_{mn}^{23}/C)) \\ +\sum_{n=1}^{N_3} sc_{mn}^{23}\sum_{a=0}^{b-1}\left[\frac{1}{2}l_{n,a} + \sum_{k=0}^{a-1} l_{n,k}\right] I_{ba}(s(R_{mn}^{23}/C)) \end{bmatrix},$$

$$S_{m,b}^{3} = -\begin{bmatrix} \begin{bmatrix} -s^2\mu\sum_{n=1}^{N_1} a_{mn}^{13}\sum_{k=0}^{b-1}(b-k)g_{n,k}^{1} I_{bb}(s(R_{mn}^{13}/C)) \\ -s^2\mu\sum_{n=1}^{N_1} a_{mn}^{13}\sum_{a=0}^{b-1}\left[\frac{1}{4}g_{n,a}^{1} + \sum_{k=0}^{a-1}(a-k)g_{n,k}^{1}\right] I_{ba}(s(R_{mn}^{13}/C)) \\ +\frac{1}{\varepsilon}\sum_{n=1}^{N_1} b_{mn}^{13}\sum_{a=0}^{b-1} g_{n,a}^{1} I_{ba}(s(R_{mn}^{13}/C)) \end{bmatrix} \\ +\begin{bmatrix} -s^2\mu\sum_{n=1}^{N_2} a_{mn}^{23}\sum_{k=0}^{b-1}(b-k)g_{n,k}^{2} I_{bb}(s(R_{mn}^{23}/C)) \\ -s^2\mu\sum_{n=1}^{N_2} a_{mn}^{23}\sum_{a=0}^{b-1}\left[\frac{1}{4}g_{n,a}^{2} + \sum_{k=0}^{a-1}(a-k)g_{n,k}^{2}\right] I_{ba}(s(R_{mn}^{23}/C)) \\ +\frac{1}{\varepsilon}\sum_{n=1}^{N_2} b_{mn}^{23}\sum_{a=0}^{b-1} g_{n,a}^{2} I_{ba}(s(R_{mn}^{23}/C)) \end{bmatrix} \\ -2\begin{bmatrix} \sum_{n=1}^{N_3} sc_{mn}^{33}\sum_{k=0}^{b-1} l_{n,k} I_{bb}(s(R_{mn}^{33}/C)) \\ +\sum_{n=1}^{N_3} sc_{mn}^{33}\sum_{a=0}^{b-1}\left[\frac{1}{2}l_{n,a} + \sum_{k=0}^{a-1} l_{n,k}\right] I_{ba}(s(R_{mn}^{33}/C)) \end{bmatrix} \end{bmatrix},$$

$$K_{m,b}^{4} = -\begin{bmatrix} -s^2\mu\sum_{n=1}^{N_1} a_{mn}^{14}\sum_{k=0}^{b-1}(b-k)g_{n,k}^{1} I_{bb}(s(R_{mn}^{14}/C)) \\ -s^2\mu\sum_{n=1}^{N_1} a_{mn}^{14}\sum_{a=0}^{b-1}\left[\frac{1}{4}g_{n,a}^{1} + \sum_{k=0}^{a-1}(a-k)g_{n,k}^{1}\right] I_{ba}(s(R_{mn}^{14}/C)) \\ +\frac{1}{\varepsilon}\sum_{n=1}^{N_1} b_{mn}^{14}\sum_{a=0}^{b-1} g_{n,a}^{1} I_{ba}(s(R_{mn}^{14}/C)) \\ -\sum_{n=1}^{N_3} sc_{mn}^{34}\sum_{k=0}^{b-1} l_{n,k} I_{bb}(s(R_{mn}^{34}/C)) \\ -\sum_{n=1}^{N_3} sc_{mn}^{34}\sum_{a=0}^{b-1}\left[\frac{1}{2}l_{n,a} + \sum_{k=0}^{a-1} l_{n,k}\right] I_{ba}(s(R_{mn}^{34}/C)) \end{bmatrix},$$

$$H_{m,b}^{4} = -\begin{bmatrix} -s^2\mu\sum_{n=1}^{N_2} a_{mn}^{24}\sum_{k=0}^{b-1}(b-k)g_{n,k}^{2} I_{bb}(s(R_{mn}^{24}/C)) \\ -s^2\mu\sum_{n=1}^{N_2} a_{mn}^{24}\sum_{a=0}^{b-1}\left[\frac{1}{4}g_{n,a}^{2} + \sum_{k=0}^{a-1}(a-k)g_{n,k}^{2}\right] I_{ba}(s(R_{mn}^{24}/C)) \\ +\frac{1}{\varepsilon}\sum_{n=1}^{N_2} b_{mn}^{24}\sum_{a=0}^{b-1} g_{n,a}^{2} I_{ba}(s(R_{mn}^{24}/C)) \\ +\sum_{n=1}^{N_3} sc_{mn}^{34}\sum_{k=0}^{b-1} l_{n,k} I_{bb}(s(R_{mn}^{34}/C)) \\ +\sum_{n=1}^{N_3} sc_{mn}^{34}\sum_{a=0}^{b-1}\left[\frac{1}{2}l_{n,a} + \sum_{k=0}^{a-1} l_{n,k}\right] I_{ba}(s(R_{mn}^{34}/C)) \end{bmatrix}.$$

REFERENCES

[1] J. Hirokawa, A. Hiroyuki, and G. Naohisa, "Cavity-backed wide slot antenna," *IEE Proceedings H (Microwaves, Antennas and Propagation), IET Digital Library*, vol. 136, no. 1, pp. 29-33, February 1989.

[2] T. Lertwiriyaprapa, C. Phongcharoenpanich, S. Kosulvit, and M. Krairiksh, "Analysis of impedance characteristics of a probe fed rectangular cavity-backed slot antenna," *IEEE Antennas and Propagation Society International Symposium, IEEE; 1999*, vol. 1, pp. 576-579, July 2001.

[3] A. Hadidi and M. Hamid, "Aperture field and circuit parameters of cavity-backed slot radiator," *IEE Proceedings H (Microwaves, Antennas and Propagation), IET Digital Library*, vol. 136, no. 2, pp. 139-146, April 1989.

[4] S. Eardprab and C. Phongcharoenpanich, "Diffraction on a rectangular aperture antenna mounted on an open-ended cavity excited by a probe," *Communications and Information Technologies, 2006, ISCIT'06, International Symposium on IEEE*, pp. 779-782, October 2006.

[5] M. V. Nesterenko, V. A. Katrich, D. Y. Penkin, S. L. Berdnik, and V. I. Kijko, "Electromagnetic waves scattering and radiation by vibrator-slot structure in a rectangular waveguide," *Progress In Electromagnetics Research M*, vol. 24, pp. 69-84, 2012.

[6] D. B. Wright, R. Lee, and D. G. Dudley, "Transient current on a wire penetrating a cavity-backed circular aperture in an infinite screen," *Electromagnetic Compatibility, IEEE Transactions on*, vol. 32, no. 3, pp. 197-204, August 1990.

[7] M. Bailin and D. K. Cheng, "Transient electromagnetic fields coupled into a conducting cavity through a slot aperture," *Scientia Sinica Series Mathematical Physical Technical Sciences*, vol. 27, pp. 775-784, July 1984.

[8] N. J. Šekeljić, A. Manić, B. M. Notaroš, and M. M. Ilić, "Transient analysis of 3D waveguides using double-higher-order time-domain finite element method," *AP-S*, 2013.

[9] Y. Zhang and M. H. Bakr, "Transient adjoint sensitivity analysis exploiting FDTD," *Microwave Symposium Digest (MTT), 2012 IEEE MTT-S*

International, IEEE, pp. 1-3, June 2012.
[10] M. Omiya, T. Hikage, N. Ohno, K. Horiguchi, and K. Itoh, "Design of cavity-backed slot antennas using the finite-difference time-domain technique," *Antennas and Propagation, IEEE Transactions on*, vol. 46, no. 12, pp. 1853-1858, December 1998.
[11] Z. Chen and S. Luo, "Generalization of the finite-difference-based time-domain methods using the method of moments," *Antennas and Propagation, IEEE Transactions on*, vol. 54, no. 9, pp. 2515-2524, September 2006.
[12] W. C. Gibson, *The Method of Moments in Electromagnetic*. CRC Press, US, 2008.
[13] M. Coghetto and C. Offelli, "A procedure for the evaluation of radiated emissions from polygonal wires with the method of moments," *Electromagnetic Compatibility, 1999 IEEE International Symposium on*, vol. 1, pp. 334-339, 1999.
[14] B. H. Jung, Y. S. Chung, and T. K. Sarkar, "Time-domain EFIE, MFIE, and CFIE formulations using Laguerre polynomials as temporal basis functions for the analysis of transient scattering from arbitrary shaped conducting structures," *Progress In Electromagnetics Research*, vol. 39, pp. 1-45, 2003.
[15] B. H. Jung, T. K. Sarkar, Y. S. Chung, M. Salazar-Palma, Z. Ji, S. Jang, and K. Kim, "Transient electromagnetic scattering from dielectric objects using the electric field integral equation with Laguerre polynomials as temporal basis functions," *Antennas and Propagation, IEEE Transactions on*, vol. 52, no. 9, pp. 2329-2340, 2004.
[16] J. Láčík and Z. Raida, "Modeling microwave structure in time domain using Laguerre polynomials," *Radioengineering*, vol. 15, no. 3, pp. 1-9, September 2006.
[17] Z. Mei, Y. Zhang, X. Zhao, B. H. Jung, T. K. Sarkar, and M. Salazar-Palma, "Choice of the scaling factor in a marching-on-in-degree time domain technique based on the associated Laguerre functions," *Antennas and Propagation, IEEE Transactions on*, vol. 60, no. 9, pp. 4463-4467, September 2012.
[18] X. Guan, S. Wang, Y. Su, and J. Mao, "A method to reduce the oscillations of solution of time domain integral equation using Laguerre polynomials," *PIERS Online*, vol. 3, no. 6, 2007.
[19] K. M. Chen, "A mathematical formulation of the equivalence principle," *IEEE Transactions on Microwave Theory and Techniques*, vol. 37, no. 10, pp. 1576-1581, October 1989.
[20] A. J. Booysen, "Aperture theory and the equivalence principle," *Antennas and Propagation Magazine, IEEE*, vol. 45, no. 3, pp. 29-40, 2003.
[21] A. J. Booysen, "Aperture theory and the equivalence theorem," *Antennas and Propagation Society International Symposium, 1999, IEEE*, vol. 2, pp. 1258-1261, July 1999.
[22] D. Omri and T. Aguili, "Time-domain techniques for electromagnetic coupling analysis of transient excitations of rectangular cavity through slot," *Journal of Electromagnetic Waves and Applications, 2015, IEEE*, vol. 29, pp. 1297-1316, April 2015.

Dorsaf Omri received the Master degree in Mathematics from Faculty of Mathematical, Physical and Natural Sciences of Tunis and the M.Sc. degree in Communication Technologies from the National Engineering School of Tunis. In 2010, she received the Ph.D. degree in Information and Communication Technologies and Sciences from the National Engineering School of Tunis. Her research interest is in the field of electromagnetic modeling and time domain numerical methods.

Taoufik Aguili received his Engineering degree in Electrical Engineering and his Ph.D. degree in Telecommunications from INSA, France. He is working as Professor at the National Engineering School of Tunis (ENIT). His research activities include electromagnetic microwave circuits modeling and analysis of scattering and propagation phenomena in free space.